Int. J. Heat Mass Transfer. Vol. 29, No. 2, pp. 169–182, 1986
Printed in Great Britain

0017–9310/86 $3.00 + 0.00
Pergamon Press Ltd.

The prediction of turbulent swirling jet flow

H. NAJI

Laboratoire de Mécanique de Lille, U.E.R. de Mathématiques Pures et Appliquées, Université de Lille I 59655 Villeneuve D'Ascq Cedex, France

(*Received* 11 *February and in final form* 8 *July* 1985)

Abstract—A space marching integration procedure is used to solve the Reynolds equations governing the axisymmetric incompressible turbulent swirling jet flow. Turbulence is modelled by the k–ε model with an isotropic turbulent viscosity. Besides mean velocity field, turbulent properties—such as Reynolds stresses, turbulent kinetic energy and dissipation rate—are obtained and the results are compared with experimental data. Agreement is quite encouraging and shows that the assumption of isotropic turbulent viscosity seems plausible.

1. INTRODUCTION

FREE AND swirling jets are of practical importance in connection with vertical-take-off aircraft and are also used in many industrial applications to effect spraying, drying, heating, coaling and leaching of liquids and solid particles. These practical cases could be managed more efficiently with the aid of swirl.

Much work has been done to predict turbulent flows numerically. Various turbulence models have been proposed to close the time-averaged governing equation system.

Unlike wall boundary layers and free shear flows such as jets and wakes, only few studies have been devoted to rotating turbulent flows [1, 2].

If there is no reverse flow present, the boundary-layer approximation is valid and the radial axis is taken as the marching direction. The governing equations are parabolic, i.e. convection phenomena are important along this direction and diffusion is effective normal to it. This leads to a particular numerical technique [3–6] which enables the so-called parabolic form of the Navier–Stokes equations to be solved. The calculation always proceeds in the downstream direction. Thus the whole flow field can be rapidly covered.

2. DEFINING THE PROBLEM

This paper is devoted to the prediction of the swirling radial free jet issuing from the gap between two parallel discs, one of them rotating at a constant rate and the other one being at rest (Fig. 1). This problem has been studied experimentally by Muhe [7, 8].

2.1. *The governing equations*

The flow is axisymmetric, so the cylindrical–polar coordinates are used.

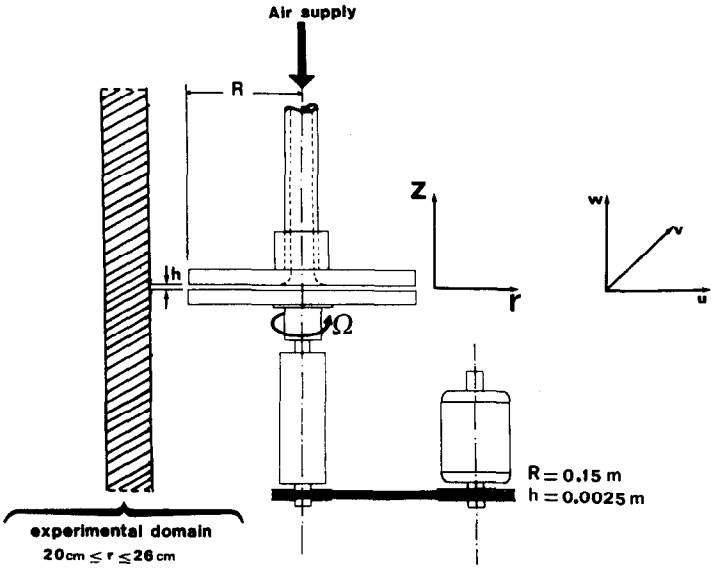

FIG. 1. Flow geometry.

NOMENCLATURE

C_ϕ total diffusion coefficient ϕ defined in equation (11) [$m^2 s^{-1}$]
D mean rate of strain tensor
F function defined by $F = W - \eta \cdot L \cdot U$
h gap width [m]
k turbulent kinetic energy $(\overline{u^2} + \overline{v^2} + \overline{w^2})/2$ [$m^{-2} s^{-2}$]
$L(r)$ length scale used in the numerical procedure [m]
P mean pressure [$N m^{-2}$]
Ps rate of shear production of k, $\overrightarrow{\text{grad}}\ \mathbf{U} \otimes 2\mathbf{D}$
Pe Péclet number, $W \cdot L \cdot \Delta\eta / C_\phi$
r, θ, z radial, angular and axial coordinates [m, rad, m]
R disc radius [m]
Re rotating Reynolds number, $\Omega \cdot R^2/\nu$
Re_t turbulent Reynolds number, $k^2/\nu \cdot \varepsilon$
S swirl parameter, $\Omega \cdot R/\bar{U}$
S_ϕ source term of variable ϕ
S_ϕ^u, S_ϕ^p linearized source terms defined in Table 1
u, v, w radial, tangential and axial fluctuating velocities [$m s^{-1}$]
U, V, W radial, tangential and axial mean velocity components [$m s^{-1}$]
$\bar{U}$ discharge exit velocity (volume flow rate/$2\pi Rh$) [$m s^{-1}$]
$\otimes$ tensorial product.

Greek symbols
δ half width of swirling jet defined from $U = U_m/2$ location [m]
Δr size of the forward step, $r^d - r^u$ [m]
ε turbulence energy dissipation rate [$m^2 s^{-3}$]
ε^* dimensionless ration, h/R
η dimensionless coordinate, $z/L(r)$
$\Delta\eta$ cross-stream size dimension of the control volume, $\eta_{j+1} - \eta_{j-1}$
η^* dimensionless coordinate, z/δ
ν, ρ kinematic viscosity and density of the fluid (air) [$m^2 s^{-1}$, $kg m^{-3}$]
ν_t kinematic turbulent viscosity defined in equation (6) [$m^2 s^{-1}$]
ϕ a general dependent variable
$\sigma_{t,\phi}$ turbulent Prandtl number for ϕ
Ω angular velocity of the rotating disc [s^{-1}].

Superscripts
d downstream station
u upstream station
$\bar{}$ mean quantities.

Subscripts
ϕ corresponding to the quantity ϕ
$+$ point at η^+
$-$ point at η^-
0 point at free stream
m maximum.

The parabolic equations governing a steady ($\partial/\partial t = 0$), axisymmetric ($\partial/\partial\theta = 0$), isothermal ($T = cte$) turbulent flow, without body forces are [9]:

$$U\frac{\partial U}{\partial r} + W\frac{\partial U}{\partial z} - \frac{V^2}{r} = -\frac{1}{\rho}\cdot\frac{\partial P}{\partial r} + \frac{\partial}{\partial z}\left(\nu\frac{\partial U}{\partial z}\right) - \frac{\partial \overline{uw}}{\partial z} \quad (1)$$

$$U\frac{\partial V}{\partial r} + W\frac{\partial V}{\partial z} + \frac{UV}{r} = \frac{\partial}{\partial z}\left(\nu\frac{\partial V}{\partial z}\right) - \frac{\partial \overline{vw}}{\partial z} \quad (2)$$

$$\frac{\partial (rU)}{\partial r} + \frac{\partial (rW)}{\partial z} = 0. \quad (3)$$

In the simplified form (1), (2) of the Navier–Stokes equations, only the r-diffusion terms are neglected.

2.2. *The two-equation turbulence model*

As (1)–(3) do not constitute a closed set of equations, it is therefore necessary to specify the quantities produced by time-averaging the non-linear convection terms: $\overline{uw}$, $\overline{vw}$. These terms are the Reynolds shear stresses.

However, the derivation of exact transport equations for these stresses leads to new partial differential equations containing higher-order turbulence unknown correlations, such as $\overline{uvw}$, etc. [10, 11].

This difficulty is generally avoided by expressing the turbulent stresses in terms of known quantities in order to obtain a closed set of equations. Turbulence models of this kind have been introduced by many authors for application to turbulent boundary-layer flows [12, 13]. Most of these models are based on the concept of turbulent or eddy viscosity ν_t.

For the radial swirling jet, the only significant Reynolds stresses are $\overline{uw}$ and $\overline{vw}$ connected to the turbulent viscosity by:

$$-\overline{uw} = \nu_t \cdot \left(\frac{\partial U}{\partial z} + \frac{\partial W}{\partial r}\right) \quad (4)$$

$$-\overline{vw} = \nu_t \cdot \left(\frac{\partial V}{\partial z}\right). \quad (5)$$

The turbulent viscosity is defined by:

$$\nu_t = C_\mu \cdot k^2/\varepsilon. \quad (6)$$

For the jet flow, the quantity C_μ is constant due to the absence of a solid wall proximity.

k and ε are obtained from the following transport equations [9, 14, 18, 19]:

$$U\frac{\partial k}{\partial r}+W\frac{\partial k}{\partial z}=\frac{\partial}{\partial z}\left[\left(\nu+\frac{\nu_t}{\sigma_k}\right)\frac{\partial k}{\partial z}\right]+\nu_t\cdot Ps-\varepsilon \quad (7)$$

$$U\frac{\partial \varepsilon}{\partial r}+W\frac{\partial \varepsilon}{\partial z}=\frac{\partial}{\partial z}\left[\left(\nu+\frac{\nu_t}{\sigma_\varepsilon}\right)\frac{\partial \varepsilon}{\partial z}\right]+C_{\varepsilon 1}\cdot\frac{\varepsilon}{k}\nu_t\cdot Ps-C_{\varepsilon 2}\cdot f_2\cdot\frac{\varepsilon^3}{k}. \quad (8)$$

According to Oliver [14] the expression of ε in cylindrical coordinates for an axisymmetric flow is:

$$\varepsilon=\nu\left\{\frac{\overline{\partial u_i}}{\partial x_j}\cdot\frac{\overline{\partial u_j}}{\partial x_i}+\frac{\overline{u^2}+\overline{v^2}}{r^2}\right\}$$

where repeated indices hold for summation over $1\leqslant i, j\leqslant 3$, and u_i is the velocity fluctuation in the direction i.

In equation (8) f_2 is a function which takes into account the low turbulent Reynolds number effects at the vicinity of the jet exit:

$$f_2=1.0-0.3\exp(-Re_t^2).$$

The different equations used here contain the quantities C_μ, $C_{\varepsilon 1}$ and $C_{\varepsilon 2}$ which in the absence of definite information, have been assumed constant for high Reynolds numbers. Their values have been taken from literature [16, 17]: $C_\mu=0.09$, $C_{\varepsilon 1}=1.45$, $C_{\varepsilon 2}=1.95$.

2.3. *Boundary conditions*

At the free-stream edge of the jet, the following conditions are employed:

$$\frac{\partial}{\partial r}(rU)|_o=0 \quad (9a)$$

$$V|_o=0 \quad (9b)$$

$$U\left.\frac{\partial k}{\partial r}\right|_o=\nu_t\cdot Ps_o-\varepsilon_o \quad (9c)$$

$$U\left.\frac{\partial \varepsilon}{\partial r}\right|_o=C_{\varepsilon 1}\cdot\frac{\varepsilon}{k}\Big|_o\nu_t Ps_o-C_{\varepsilon 2}\cdot f_2\cdot\left.\frac{\varepsilon^2}{k}\right|_o. \quad (9d)$$

The subscript o specifies outer conditions. The first condition (9a) implies that U at $z=z_o$ can be different to zero even though this is not reported in Fig. 5. Moreover, $U^d=r^u\cdot U^u/r^d$ with the outer velocity at $r^u=R$ is one hundredth of the core flow velocity $\bar{U}$. Equations (9c) and (9d) are the reduced forms of equations (7) and (8) by setting the transverse gradients to be zero [3, 6].

3. NUMERICAL PROCEDURE

Equations (1)–(3), (7) and (8) together with the boundary conditions (9) form a closed set of equations. These equations may be written in a unified form:

$$\frac{\partial}{\partial r}(rU\phi)+\frac{\partial}{\partial z}(rW\phi)=r\cdot\frac{\partial}{\partial z}\left(C_\phi\cdot\frac{\partial \phi}{\partial z}\right)+r\cdot S_\phi \quad (10)$$

where $\phi=(U, V, k, \varepsilon)$. S_ϕ is the source rate of the averaged quantity ϕ and C_ϕ stands for the diffusion coefficient which can be expressed by:

$$C_\phi=\nu+\frac{\nu_t}{\sigma_{t,\phi}}. \quad (11)$$

The values assigned to $\sigma_{t,\phi}$ are [15]: $\sigma_{t,\phi}=1$ for $\phi=U, V, k$ and $\sigma_{t,\phi}=1.3$ for $\phi=\varepsilon$.

3.1. *Transformed coordinate system*

Since the domain of the jet flow grows with the radial distance and since the transverse flow velocity is generally very small, it is inconvenient to discretize the original differential equation (10). As a consequence, we introduce a length scale $L(r)$ and we transform the physical plane r, z (Fig. 2a) into the r, η plane, where

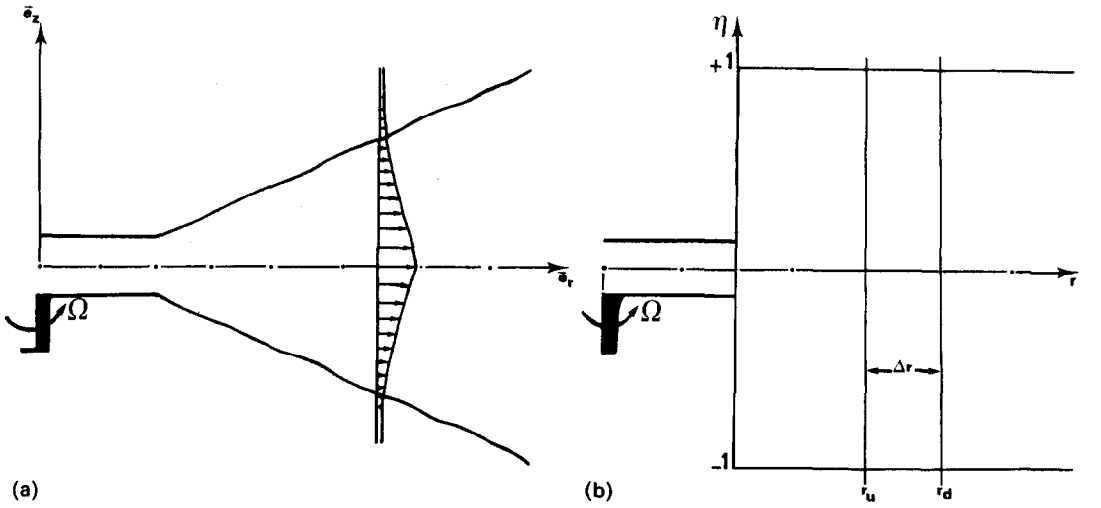

FIG. 2. Physical and calculation domain.

η is the dimensionless coordinate defined by:

$$\eta = z/L(r). \tag{12}$$

A linear variation has been prescribed for $L(r)$ according to experimental data.

The transformed domain is of rectangular geometry (Fig. 2b).

3.2. *Transformed differential equations*

Using the variables r, η, equations (3) and (10) are now formulated as:

$$\frac{\partial(rU)}{\partial r} - r\frac{\dot{L}}{L}\eta\frac{\partial U}{\partial \eta} + \frac{r}{L}\cdot\frac{\partial W}{\partial \eta} = 0 \tag{13}$$

$$\frac{1}{L}\cdot\frac{\partial(rW\phi)}{\partial \eta} + \frac{\partial(rU\phi)}{\partial r} - \frac{\dot{L}}{L}\eta\frac{\partial(rU\phi)}{\partial \eta} = \frac{r}{L^2}\cdot\frac{\partial}{\partial \eta}\left(C_\phi\frac{\partial \phi}{\partial \eta}\right) + rS_\phi \tag{14}$$

where $\dot{L} = \mathrm{d}L/\mathrm{d}r$.

In order to overcome the non-linearity of S_ϕ, we express it as [4]:

$$S_\phi = S_\phi^{\mathrm{u}} + S_\phi^{\mathrm{p}}\cdot\phi. \tag{15}$$

The definition of S_ϕ^{u} and S_ϕ^{p} are given in Table 1.

By an order-of-magnitude analysis we can show that the quantity $C_{\varepsilon 1}v_{\mathrm{t}}\cdot Ps - C_{\varepsilon 2}\cdot f_2\cdot\varepsilon$ is less than or equal to zero except possibly in the neighbourhood of δ. Therefore, the source term S_ϕ^{p} is not positive.

The details of procedure for linearizing the source terms can be found in ref. [4].

Before starting discretization of the above equations, they can recast in a different form by introducing the function $F = W - \eta\cdot L\cdot U$:

$$\frac{\partial(rU)}{\partial r} + \frac{r}{L}\cdot\frac{\partial F}{\partial \eta} + \frac{\dot{L}}{L}rU = 0 \tag{16}$$

$$\frac{\partial(rU\phi)}{\partial r} + \frac{1}{L}\cdot\frac{\partial}{\partial \eta}(r\cdot F\cdot\phi) = \frac{r}{L^2}\cdot\frac{\partial}{\partial \eta}\left(C_\phi\cdot\frac{\partial \phi}{\partial \eta}\right) + r\left\{S_\phi^{\mathrm{u}} + \left(S_\phi^{\mathrm{p}} - \frac{\dot{L}}{L}U\right)\phi\right\}. \tag{17}$$

3.3. *Discretization*

The basic assumptions which are required for integration over the control volume are identical to those formulated by Patankar and Spalding [3]. Figure 3 shows part of a finite-difference grid where the values of ϕ are assumed known. So we get:

$$(r^{\mathrm{d}}U_j^*\phi_j^{\mathrm{d}} - r^{\mathrm{u}}U_j^{\mathrm{u}}\phi_j^{\mathrm{u}})\Delta\eta + \frac{r\cdot\Delta r}{L^{\mathrm{d}}}\{[\max({}_+F_+^{\mathrm{u}}, 0) + \max({}_-F_-^{\mathrm{u}}, 0)]\phi_j^{\mathrm{d}} - \phi_{j+1}^{\mathrm{d}}\cdot\max({}_-F_+^{\mathrm{u}}, 0) - \phi_{j-1}^{\mathrm{d}}\cdot\max({}_+F_-^{\mathrm{u}}, 0)\} - \{S_\phi^{\mathrm{u}} + [S_\phi^{\mathrm{p}} - (\dot{L}/L)^{\mathrm{u}}U_j^{\mathrm{u}}]\phi_j^{\mathrm{d}}\}\bar{r}\cdot\Delta r\cdot\Delta\eta - \frac{\bar{r}\cdot\Delta r}{L^{\mathrm{d}}}\left\{\frac{C_\phi^{\mathrm{u}}}{L^{\mathrm{d}}\cdot\Delta\eta_+}\cdot G\left(\frac{F_+^{\mathrm{u}}\cdot L^{\mathrm{d}}\cdot\Delta\eta_+}{C_{\phi_+}^{\mathrm{u}}}\right)(\phi_{j+1}^{\mathrm{d}} - \phi_j^{\mathrm{d}}) - \frac{C_{\phi_+}^{\mathrm{u}}}{L^{\mathrm{d}}\cdot\Delta\eta_-}\cdot G\left(\frac{F_-^{\mathrm{u}}\cdot L^{\mathrm{d}}\cdot\Delta\eta_-}{C_{\phi_+}^{\mathrm{u}}}\right)(\phi_j^{\mathrm{d}} - \phi_{j-1}^{\mathrm{d}})\right\} = 0 \tag{18}$$

where $\Delta\eta_+ = \eta_{j+1} - \eta_j$ and $\Delta\eta_- = \eta_j - \eta_{j-1}$.

The details of the discretization are given in ref. [9].

In the first term of equation (18) U^* is unknown and must be estimated from the continuity equation in order to linearize the convection terms [5].

When using the hybrid scheme [4], the terms of diffusion in equation (18) are multiplied by a function G of the Péclet number Pe which is defined by:

$$G(Pe) = \max(0.0, 1 - 0.5|Pe|). \tag{19}$$

The Péclet number accounts for the convection and diffusion fluxes through the boundaries of the control volume.

3.4. *The continuity equation*

The continuity equation (16) is discretized at node η_j in order to compute W at the downstream location. The result is:

$$W_+ = W_- - \frac{L^{\mathrm{d}}}{\bar{r}\cdot\Delta r}\cdot\Delta\eta(r^{\mathrm{d}}U_j^{\mathrm{d}} - r^{\mathrm{u}}U_j^{\mathrm{u}}) + \dot{L}^{\mathrm{d}}\eta_j(U_{j+1}^{\mathrm{d}} - U_{j-1}^{\mathrm{d}})/2. \tag{20}$$

Table 1. Linearized source terms

ϕ	S_ϕ^{u}	S_ϕ^{p}
U	$\frac{V^2}{r} - \frac{1}{\rho}\cdot\frac{\partial P}{\partial r}$	0
V	$-\frac{UV}{r}$	0
k	$v_{\mathrm{t}}\rho_{\mathrm{d}} - \varepsilon$	0
ε	0	$1/k(C_{\varepsilon 1}v_{\mathrm{t}}\cdot Ps - f_2\cdot C_{\varepsilon 2}\cdot\varepsilon)$

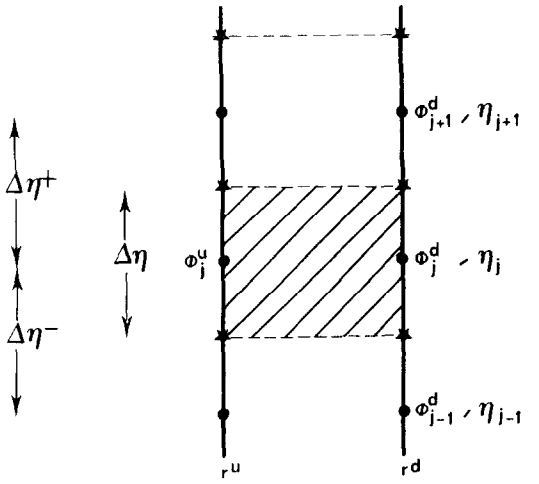

FIG. 3. Control volume.

3.5. *Solution procedure*

The resulting discretized equations (18) are solved by using a classical substitution technique of Thomas for inversion of tridiagonal matrices [20–22].

The calculation domain is covered by a rectangular mesh with a non-uniform cell size such that the grid is very fine near the discs in the z and r directions. Figure 4 shows the grid which has been used to perform the calculations.

3.6. *Conditions at the exit*

Starting profiles for velocity and turbulent quantities are taken from results due to a computation of the flow field between the discs [9]. These profiles are plotted on Fig. 5 vs the axial dimensionless variable η^* for different values of S and for $r/h = 60$.

4. PREDICTION AND DISCUSSION

The calculated values of the various dependent variables are presented together with experimental data coming from refs. [7] and [8].

In order to make a comparison with the experimental data, the obtained predictions have been reduced to represent the following characteristics: dimensionless velocity profiles U/U_m and V/V_m, radial and tangential decay of maximum velocity, dimensionless turbulent shear stresses $\overline{uw}/U_m^2$ and $\overline{vw}/U_m^2$.

4.1. *Dimensionless velocity profiles*

The dimensionless velocity profiles U/U_m are compared for different values of S, and for two radial positions $r/h = 80$ and $r/h = 104$ (Figs. 6a and b). It can be seen that the calculation is in good agreement with the experimental data except for $|\eta^*| > 1.6$ because in this zone, the measurement by hot-wire anemometers are so difficult and this explains the absence of the experimental results for $|\eta^*| > 1.6$.

The tangential mean velocity is plotted in Figs. 7a and b. The agreement with experimental results is quite good for $|\eta^*| \leqslant 0.4$, while for $|\eta^*| > 0.4$ the standard k–ε model overestimates the calculated profiles with respect to the experimental ones. The discrepancy could stem from either the measured values of V by hot-wire anemometers at low velocities [23] or from the ε-equation [24, 25].

4.2. *Characteristic scales*

In Figs. 8 and 9 the variation of the predicted and measured radial and tangential maximum mean velocity are compared. The agreement is very satisfactory.

The comparison between the measured and

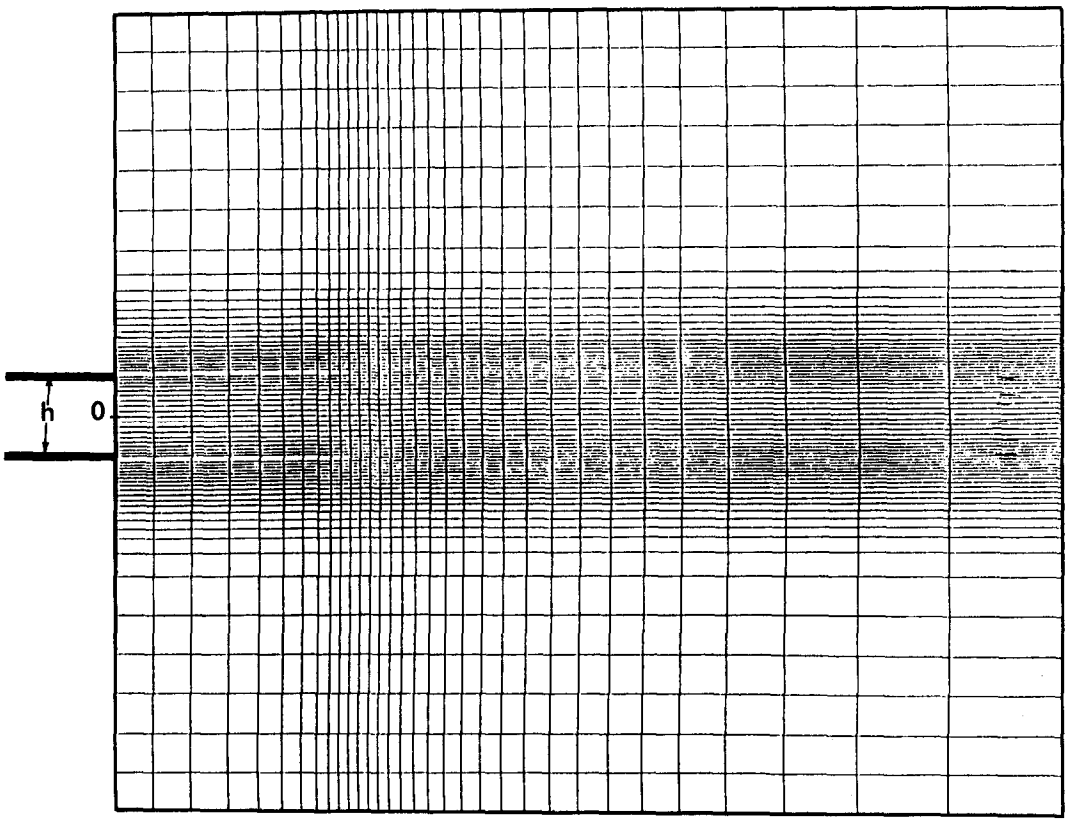

FIG. 4. Calculation grid.

s	k−ϵ	U_m
1.67	●	27.76
2.90	△	21.60
3.33	□	27.80
4.16	×	20.93

(a)

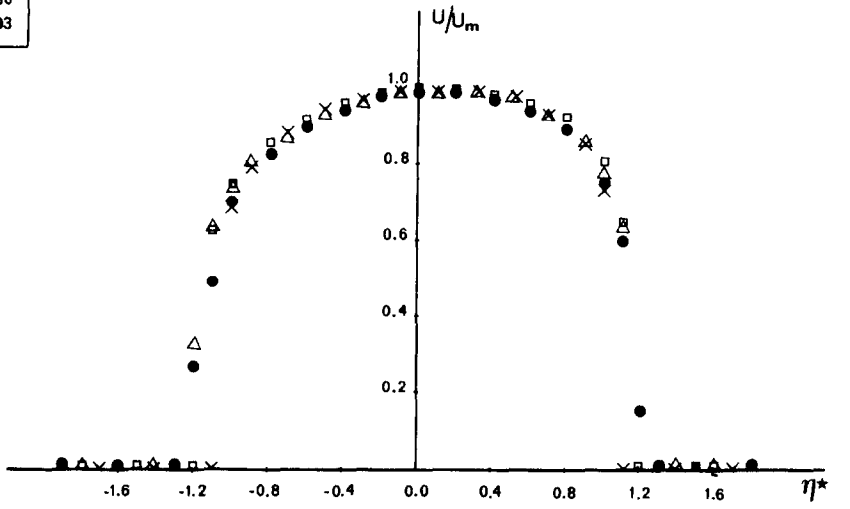

s	k − ϵ	V_m
1.67	●	39.27
2.90	△	54.94
3.33	□	78.50
4.16	×	78.50

(b)

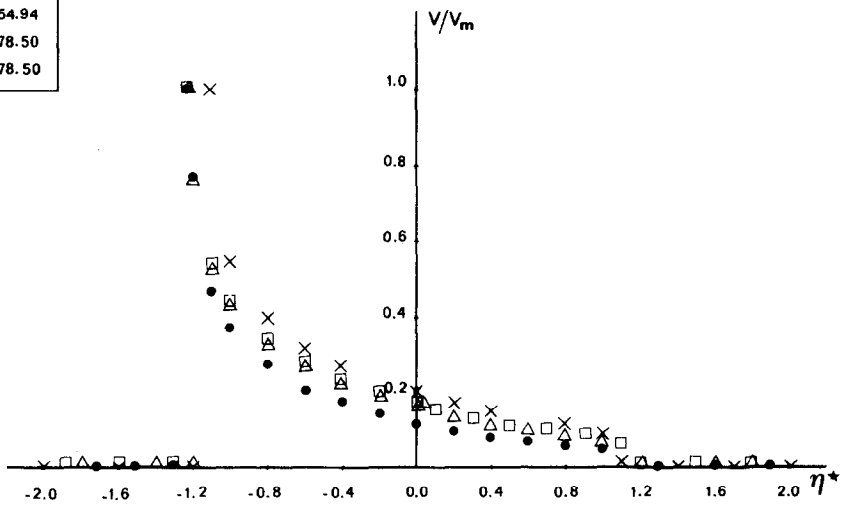

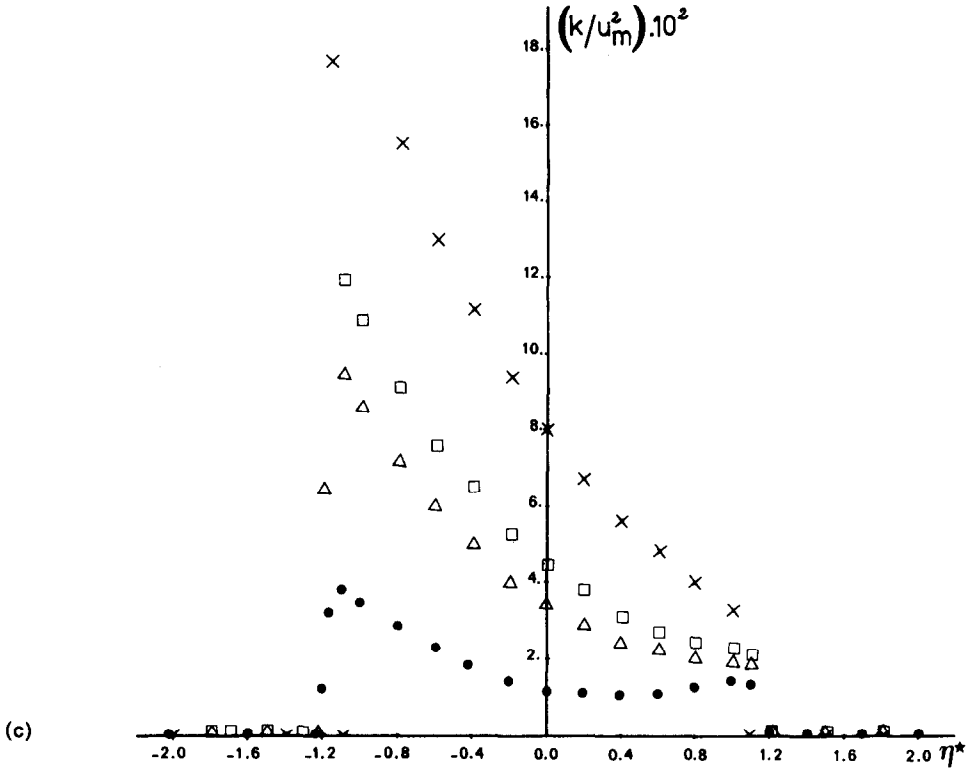

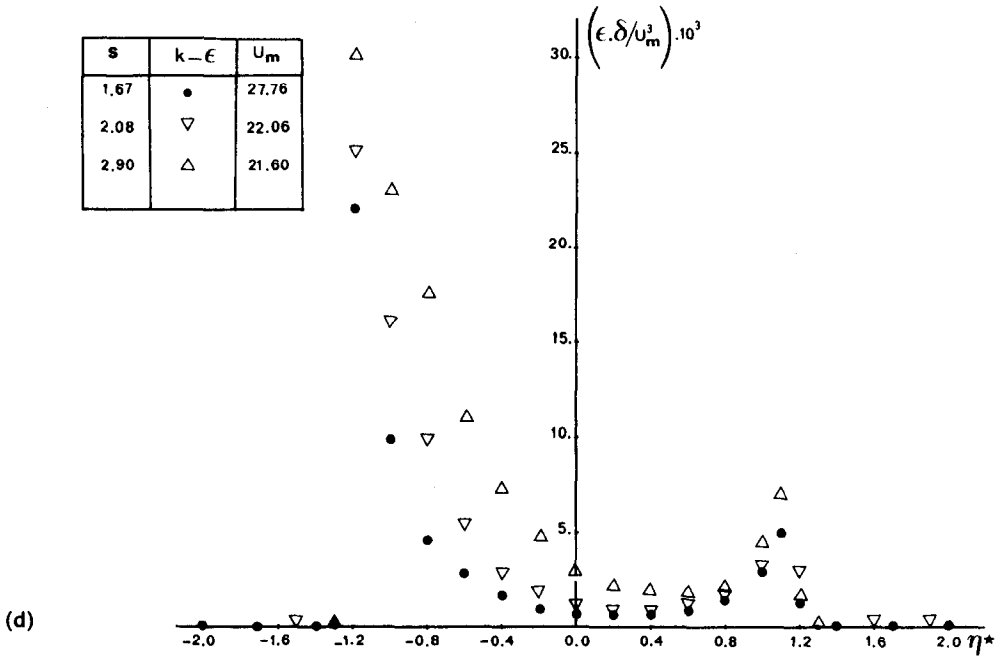

FIG. 5. Initial profiles of (a) U, (b) V, (c) k and (d) ε at $r/h = 60$.

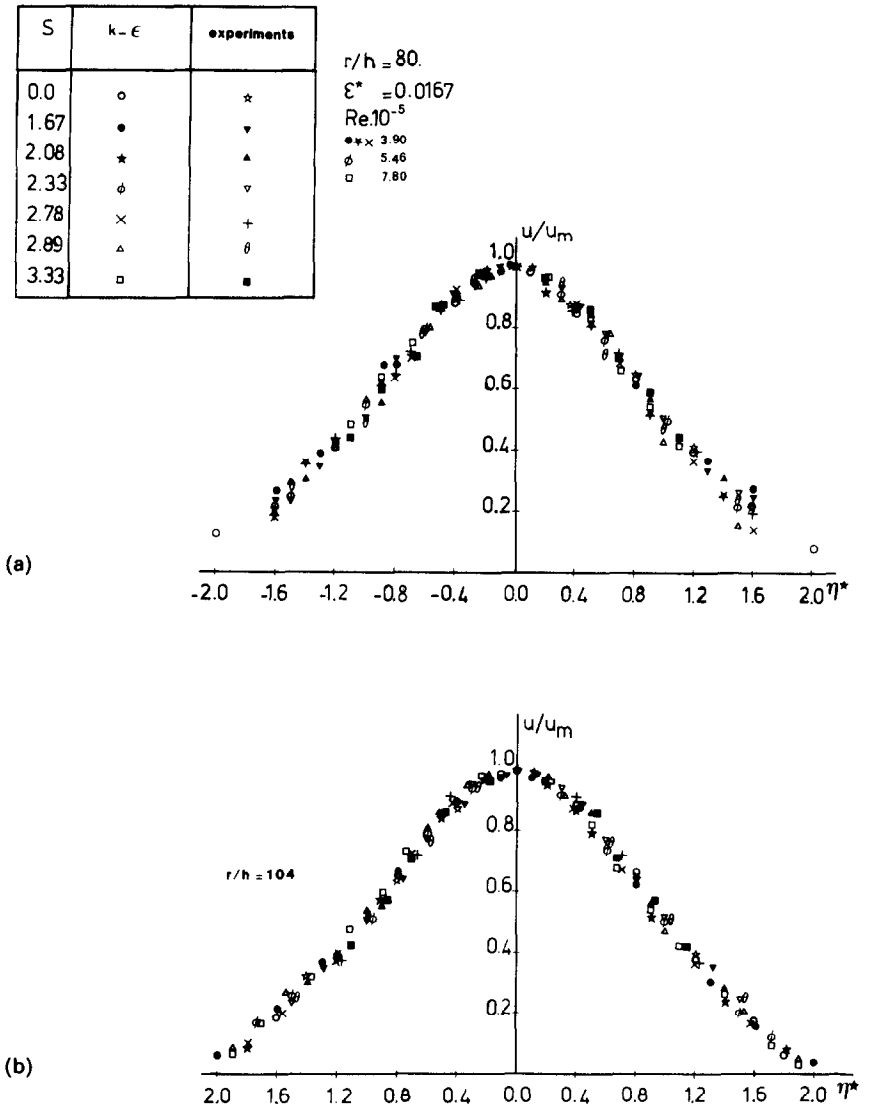

FIG. 6. Axial distribution of radial mean velocity U.

calculated value of the local degree of swirl, i.e. the ratio V_m/U_m, plotted in Fig. 10, shows also that the agreement is quite good except for the lowest values of S and r/h.

Figure 11 compares the calculated and measured jet spreading rates. The agreement is not very good. Indeed, experiments show that the jet spreads linearly with r, whereas the calculations predict effectively the linearity of the growth but with slightly different slopes.

A survey of this figure shows that the numerical prediction enables us to obtain a virtual origin of the jet independent on S and located between $r/h = 50$ and $r/h = 60$, while experiments show that for high values of S the virtual origins is located between $r/h = 20$ and $r/h = 40$.

4.3. *Turbulence characteristics*

The curves plotted in Fig. 12a, b and c give the turbulent shear stress $\overline{uw}$ scaled by U_m^2. Results are presented for three values of r/h and different values of S. Continuous and broken lines are present predictions and symbols measurements [8]. The prediction is correct, except in the intermittent region of the jet where the k–ε model leads to an overestimation of the Reynolds shear stress $\overline{uw}$.

The turbulent shear stress $\overline{vw}$ is presented in the same manner in Figs. 13a, b and c. The k–ε model provides similar profiles for all values of S, while experiments obtain this result only for high values of S. We will notice that for high values of S the prediction is correct and that for $\eta^* > 0$ (respectively $\eta^* < 0$) $\overline{vw}$ is overestimated (respectively underestimated) by the model. The discrepancy between the numerical and experimental results may be due to the model which connects the shear stress to the mean velocity gradient via the eddy viscosity concept.

Profiles of k and ε are not included for discussion

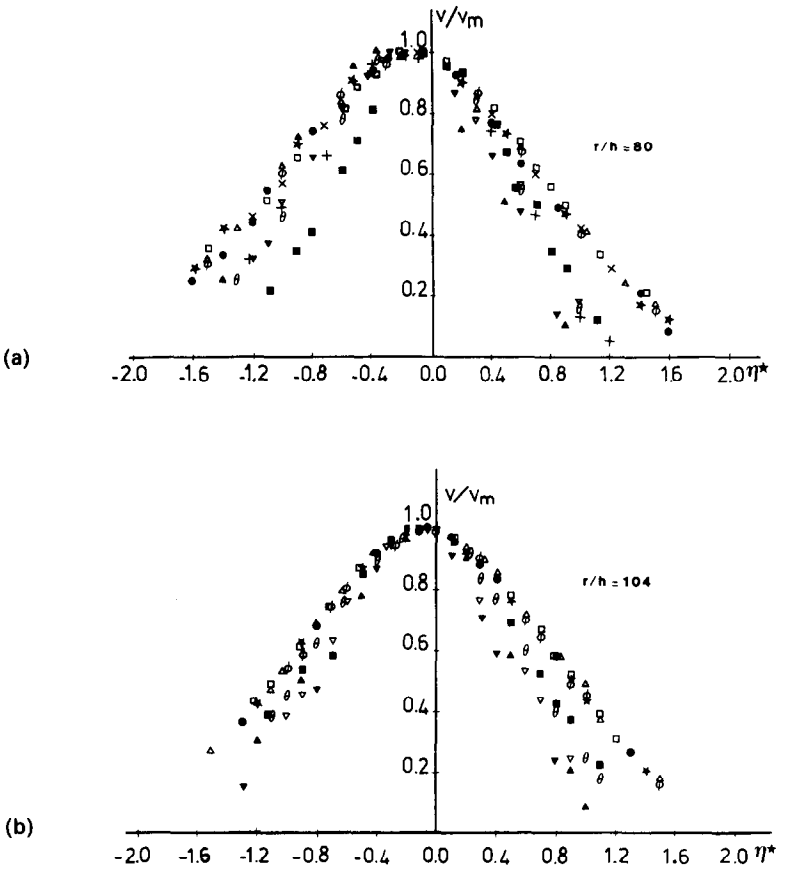

FIG. 7. Axial distribution of tangential mean velocity V.

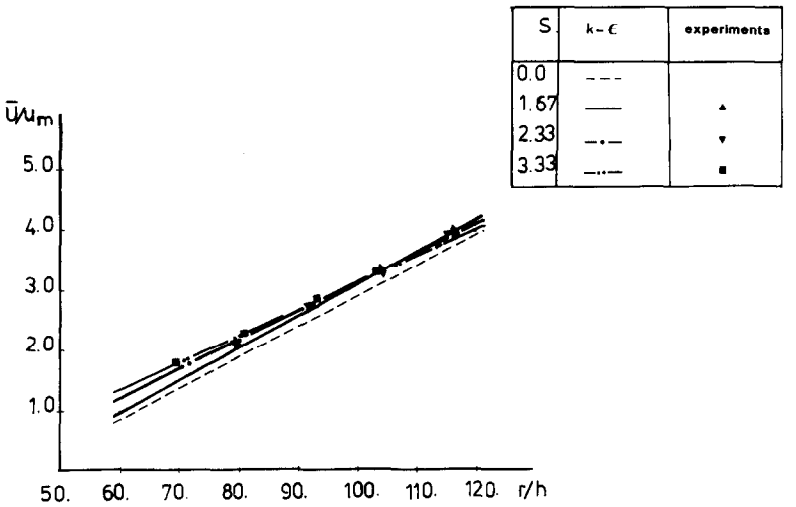

FIG. 8. Radial decay of the radial maximum mean velocity U_m.

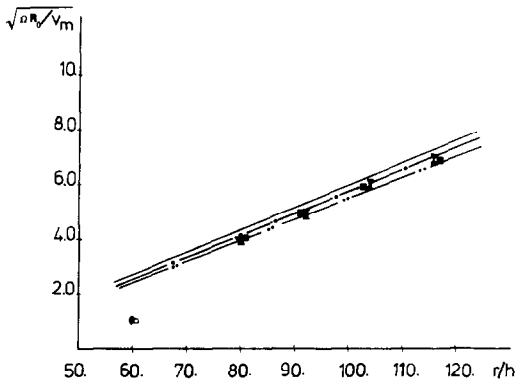

FIG. 9. Radial decay of the tangential maximum mean velocity V_m.

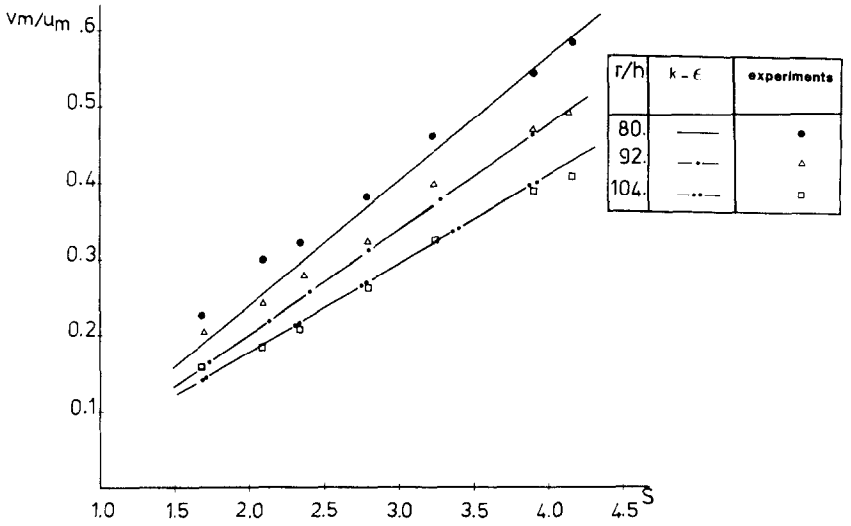

FIG. 10. Variation of the local degree of swirl with swirl parameters S.

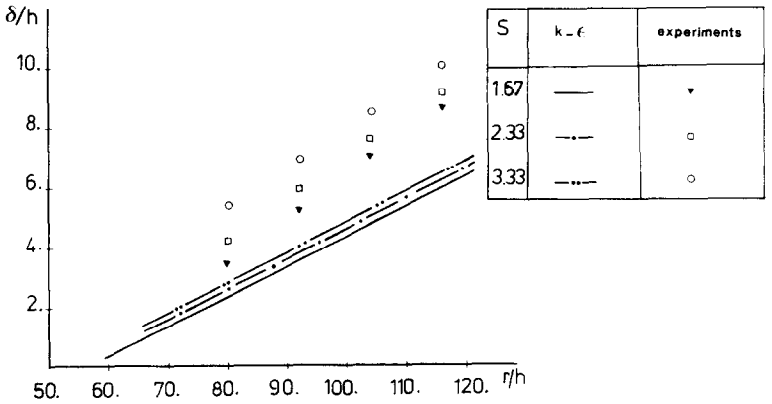

FIG. 11. Jet spreading with r/h.

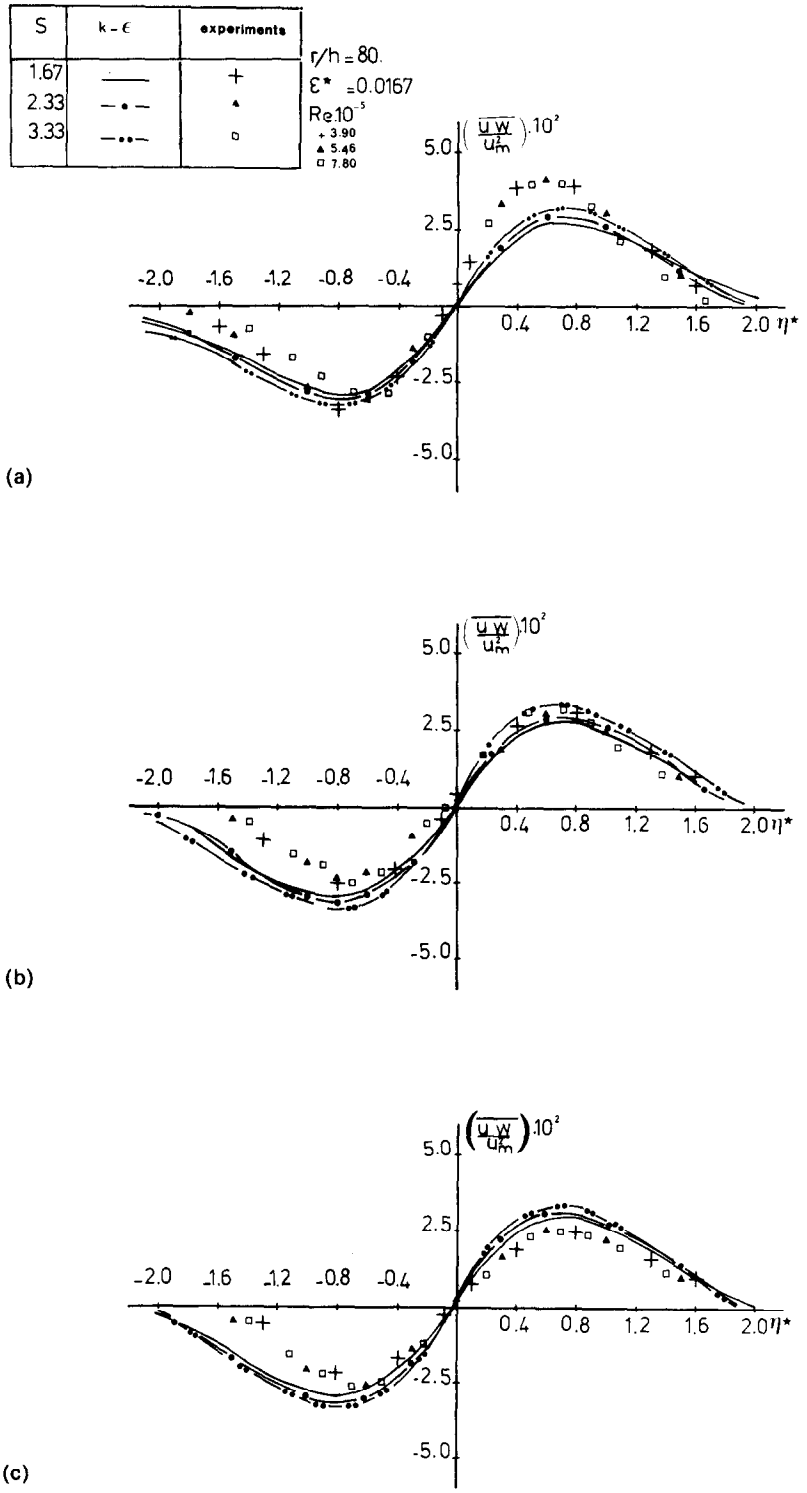

FIG. 12. Axial distribution of $\overline{uw}$ profiles. (a) $r/h = 80$, (b) $r/h = 92$, (c) $r/h = 104$.

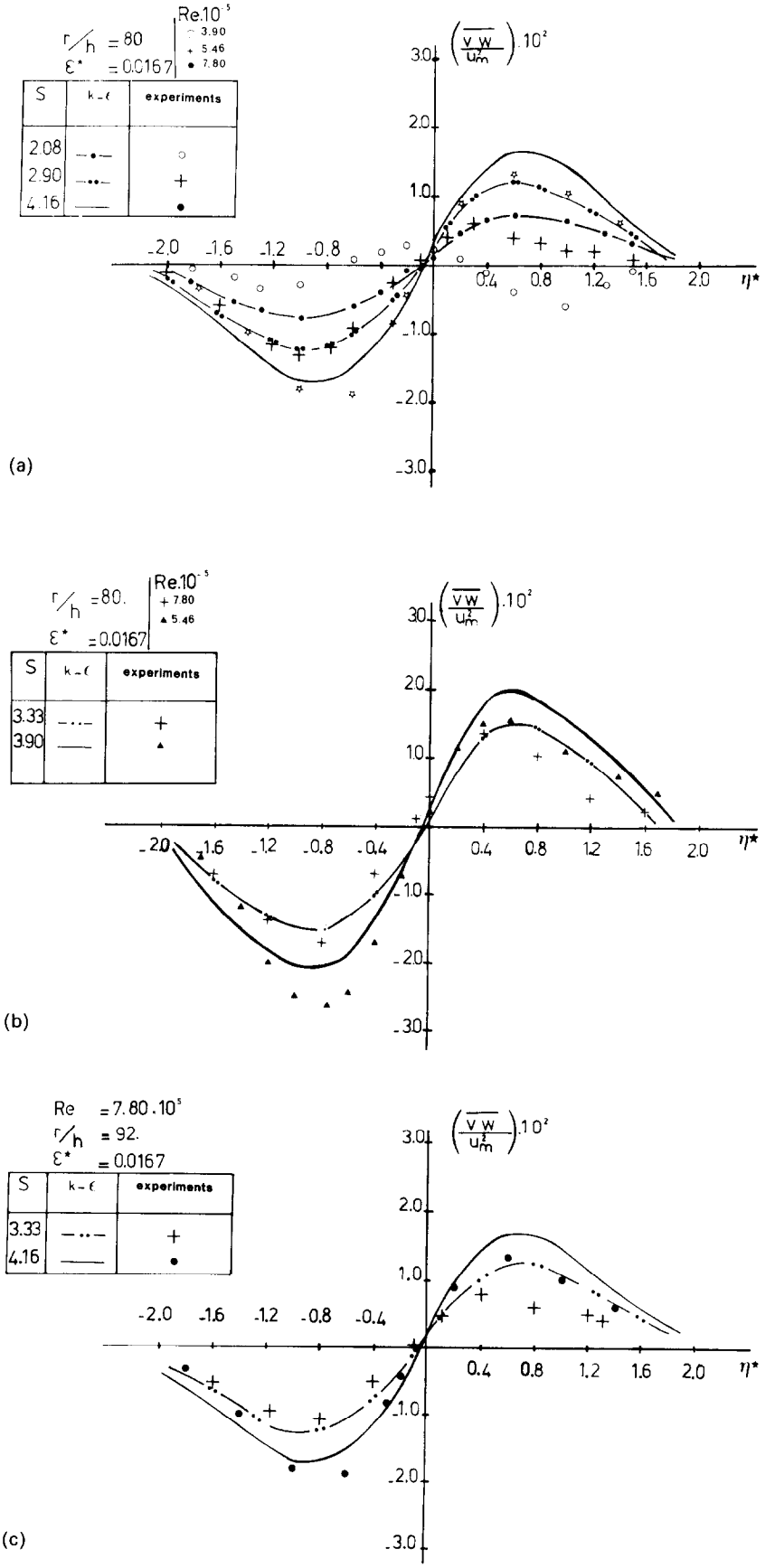

FIG. 13. Evolution axial distribution of $\overline{vw}$ profiles. (a) $r/h = 80$, (b) $r/h = 80$, (c) $r/h = 92$.

since, in the absence of relevant experimental data, no comparisons were possible. They can be found in ref. [9].

5. CONCLUSIONS

The study reported herein has shown that axisymmetric swirling flows such jets can be numerically investigated by the numerical method developed in ref. [3].

For large radial distance, experiments show that the maximum radial and tangential mean velocity vary asymptotically as $1/r$ and $1/r^2$ and computational predictions corroborate this result.

The jet thickness is found to be a linear function of the downstream distance both experimentally and numerically, but the calculated spreading rate is smaller than the experimental one. The discrepancy probably comes from the ε-equation which is not entirely adequate for rotating flows [24–26].

Nevertheless, the overall observation of predictions implies that the performance of a simple k–ε model seems to be encouraging.

Concerning future developments, there are several areas in which further research is necessary. The first is to modify the ε-equation for swirling flows by making $C_{\varepsilon 2}$ a function of the gradient Richardson number [25]. The second is to use a spectral model like that of Hanjalic *et al.* [26] and Launder *et al.* [27]. The third is the need for additional experimental data, especially for the distributions of V and $\overline{vw}$ which will enable refinement of the turbulence model.

Acknowledgments—The assistance of Drs J. Cousteix and R. Houdeville of C.E.R.T.-O.N.E.R.A. for computations is greatly acknowledged. The author is grateful to Drs D. Vandromme and H. Muhe for their helpful discussion. Thanks are due also to Professor A. Dyment for his encouragements.

REFERENCES

1. A. D. Gosman, F. C. Lockwood and J. N. Loughead, Prediction of recirculating, swirling, turbulent flow in rotating disc systems, *J. mech. Engng Sci.* 142–148 (1976).
2. D. G. Lilley, Prediction of inert turbulent swirl flows, *AIAA J.* **11**, 955–960 (1973).
3. S. V. Patankar and D. B. Spalding, *Heat and Mass Transfer in Boundary Layer*, 2nd edn. Intertext, London (1970).
4. S. V. Patankar, *Numerical Heat Transfer and Fluid Flow*, Series in Computational Methods in Mechanics and Thermal Sciences, McGraw-Hill, New York (1980).
5. J. Cousteix, X. De Saint Victor and R. Houdeville, Marching methods to solve the Navier–Stokes equations in two and three-dimensional flows, Third Symposium on Numerical and Physical Aspects of Aerodynamics Flows, State University, Long Beach, California (1985).
6. D. Vandromme, Contribution à la modélisation et à la prédiction d'écoulements turbulents à masse volumique variable. Thèse d'Etat, Université de Lille, France (1983).
7. H. Muhé, Jets tournants libre et pariétal. Thèse de Docteur Ingénieur, Université de Lille, France, (1982).
8. H. Muhé, The swirling radial jet, Structure of complex turbulent shear flow. In *IUTAM Symposium*, Marseille. Springer-Verlag, Berlin (1982).
9. H. Naji, Modélisation et calcul de l'écoulement turbulent dans un jet tournant. Thèse de Docteur de 3ème cycle, Université de Lille, France (1984).
10. K. Hanjalic and B. E. Launder, A Reynolds stress model of turbulence and its application to thin shear flows, *J. Fluid Mech.* **52**, 609–638 (1972).
11. B. E. Launder, G. H. Reece and W. Rodi, Progress in the development of a Reynolds stress turbulence closure, *J. Fluid Mech.* **68**, 537–566 (1975).
12. B. E. Launder and D. B. Spalding, *Mathematical Models of Turbulence*. Academic Press, New York (1972).
13. B. E. Launder and D. B. Spalding, Numerical computation of turbulent flows, *Comput. Meth. Appl. Mech. Engng* **3**, 269–289 (1974).
14. A. J. Oliver, The prediction of heat transfer and fluid flow in the entrance region of an annulus with the inner cylinder rotating. Ph.D. thesis, Central Electricity Research Laboratories, Leatherhead, Surrey, U.K. (1975).
15. A. Pollard, Flows in tee-junctions. Ph.D. thesis, University of London (1978).
16. B. E. Launder, A. D. Morse, W. Rodi and D. B. Spalding, The prediction of free shear flows—a comparison of the performance of six turbulence models, *Proc. Langley Free Shear Flows Conference*, Vol. 1 (1972).
17. B. E. Launder, Progress in the modelling of turbulent transport, Lecture series 76, Prediction methods for turbulent flows, V. K. Institute (1975).
18. W. Rodi, Basic equations for turbulent flow in cartesian and cylindrical coordinates, Imperial College Report, BL/TN/A/36 (1970).
19. W. Rodi, On the equation governing the rate of turbulence energy dissipation, Imperial College Report, TM/TN/A/14 (1971).
20. P. J. Roache, *Computational Fluid Dynamics*. Hermosa, Albuquerque, NM (1972).
21. R. D. Ritchmeyer and K. W. Morton, *Difference Methods for Initial Value Problem*, 2nd edn. Intertext, London (1967).
22. T. M. Shih, *Numerical Heat Transfer*, series in computational methods in mechanics and thermal sciences. Hemisphere, Washington, DC (1984).
23. A. Baille, Lois de refroidissement des fils chauds à faibles vitesses, Bulletin de la Direction des Etudes et Recherches, E.D.F., France No. 3 (1973).
24. B. E. Launder and A. Morse, Numerical prediction of axisymmetric free shear flows with a Reynolds stress closure. In *Turbulent Shear Flows*. Springer-Verlag, Berlin (1979).
25. W. Rodi, Influence of bouyancy and rotation on equations for the turbulent length scale, *2nd Symp. Turbulent Shear Flows*, pp. 10.37–10.42 (1979).
26. K. Hanjalic, B. E. Launder and R. Schiestel, Multiple-time scale concepts in turbulent transport modelling, *2nd Symp. Turbulent Shear Flows*, pp. 10.30–10.36 (1979).
27. B. E. Launder and R. Schiestel, Application d'un modèle de turbulence à échelles multiples au calcul d'écoulements libres turbulents, *C.r. Acad. Sci. Paris* **288**, 127–130 (1979).

PREDETERMINATION D'UN ECOULEMENT DE JET TOURNANT TURBULENT

Résumé—Une procédure de calcul pas à pas a été prise comme base de résolution numérique des équations de Reynolds gouvernant l'écoulement turbulent dans un jet tournant. Le caractère turbulent a été pris en compte par une modélisation simple basée sur le concept d'une viscosité turbulente dont la détermination a été réalisée à l'aide du modèle k–ε. Le calcul a permis de déterminer, en plus des profils de vitesses moyennes, les tensions de Reynolds, l'énergie cinétique de turbulence et son taux de dissipation. L'accord avec les résultats expérimentaux est relativement satisfaisant et montre que l'utilisation d'une viscosité turbulente isotropique semble correcte.

DIE BERECHNUNG DER STRÖMUNG EINES TURBULENTEN ROTIERENDEN STRAHLS

Zusammenfassung—Eine räumlich fortschreitende Integrationsmethode wurde verwendet, um die Reynolds'schen Gleichungen zu lösen, welche die achsensymmetrische, inkompressible, turbulente Strömung eines rotierenden Strahls beschreiben. Als Turbulenzmodell wurde das k–ε-Modell mit isotroper turbulenter Viskosität gewählt. Außer dem mittleren Geschwindigkeitsfeld wurden die turbulenten Eigenschaften, wie z. B. Reynolds'sche Schubspannung, kinetische Turbulenzenergie sowie die Dissipationsrate, berechnet. Die Ergebnisse wurden mit experimentellen Daten verglichen. Die Übereinstimmung ist relativ gut und zeigt, daß die Annahme einer isotropen turbulenten Viskosität gerechtfertigt erscheint.

РАСЧЕТ ТУРБУЛЕНТНОГО ЗАКРУЧЕННОГО СТРУЙНОГО ПОТОКА

Аннотация—Используется метод пространственного интегрирования для решения уравнений Рейнольдса, описывающих осесимметричное несжимаемое турбулентное закрученное струйное течение. Используется k–ε модель с изотропной турбулентной вязкостью. Помимо распределения осредненных скоростей определены такие характеристики турвулентности, как напряжения Рейнольдса, турбулентная кинетическая энергия и скорость диссипации. Проведено сравнение с экспериментальными данными и получено обнадеживающее соответствие. Показано, что допущение об изотропной турбулентной вязкости является вполне оправданным.